Geomechanics and Engineering, *Vol. 11, No. 6 (2016) 739-756*
DOI: http://dx.doi.org/10.12989/gae.2016.11.6.739

A modified shear strength reduction finite element method for soil slope under wetting-drying cycles

Yiliang Tu [1,2], Zuliang Zhong [*1,2,3], Weikun Luo [1,2], Xinrong Liu [1,2] and Sui Wang [1,2]

[1] *College of Civil Engineering, Chongqing University, Chongqing 400045, China*
[2] *Key Laboratory of New Technology for Construction of Cities in Mountain Area (Chongqing University), Ministry of Education, Chongqing, 400045, China*
[3] *Department of Architecture and Civil Engineering, Logistical Engineering University, Chongqing, 400041, China*

(*Received December 13, 2014, Revised June 02, 2016, Accepted July 09, 2016*)

Abstract. The shear strength reduction finite element method (SSRFEM) is a powerful tool for slope stability analysis. The factor of safety (FOS) of the slope can be easily calculated only through reducing effective cohesion (c') and tangent of effective friction angle ($\tan\varphi'$) in equal proportion. However, this method may not be applicable to soil slope under wetting-drying cycles (WDCs), because the influence of WDCs on c' and $\tan\varphi'$ may be different. To research the method of estimating FOS of soil slopes under WDCs, this paper presents an experimental study firstly to investigate the effects of WDCs on the parameters of shear strength and stiffness. Twelve silty clay samples were subjected to different number of WDCs and then tested with triaxial test equipment. The test results show that WDCs have a degradation effect on shear strength $(\sigma_1 - \sigma_3)_f$, secant modulus of elasticity (E_s) and c' while little influence on φ'. Hence, conventional SSRFEM which reduces c' and $\tan\varphi'$ in equal proportion cannot be adopted to compute the FOS of slope under conditions of WDCs. The SSRFEM should be modified. In detail, c' is merely reduced among shear strength parameters, and elasticity modulus is reduced correspondingly. Besides, a new approach based on sudden substantial changes in the displacement of marked nodes is proposed to identify the slope failure in SSRFEM. Finally, the modified SSRFEM is applied to compute the FOS of a slope example.

Keywords: wetting-drying cycles; shear strength reduction finite element method; modification; factor of safety; soil slope

1. Introduction

In nature, there are three kinds of wetting-drying cycles (WDCs): seasonal variation in rainfall, groundwater migration cycles and rising-falling cycles of reservoir water level (Nowamooz *et al*. 2013). It is now widely accepted that WDCs can affect the mechanical properties of geomaterials that determine the factor of safety (FOS) of slope (Aldaood *et al*. 2014 and Kampala *et al*. 2014). Kilsby *et al*. (2009) summarized some of the evidence that suggests WDCs do have an effect on behaviour of infrastructure slopes. Many soil slopes were damaged by such environment and that the losses were heavy (Mshana *et al*. 1993, Leroueil 2001, Guney *et al*. 2007 and Al-Mukhtar *et al*. 2012). Therefore, it is of great significance to study the stability of soil slope under WDCs.

*Corresponding author, Professor, E-mail: haiou983@126.com

http://www.techno-press.org/?journal=gae&subpage=7 ISSN: 2005-307X (Print), 2092-6219 (Online)

Currently, some studies have been carried out. On the one hand, the in-situ test and laboratory test are preferred by engineers and researchers. Hughes *et al*. (2009) provided data related to the failure modes and sustainability of UK infrastructure slopes anticipated as a result of climate of WDCs. The water content, which affects the stability of clay slope in England, is analyzed by Toll *et al*. (2008) and Clarke and Smethurst (2010) under conditions of WDCs. Brooks *et al*. (2004) combined field and modelling approaches to establish threshold rainfall totals that trigger shallow landslides in climate of WDCs in deforested hill country of New Zealand. Gullà *et al*. (2006) investigated the effects of the WDCs on the compressibility and shear strength of a natural clay in the superficial layers. On the other hand, the numerical technique is also an effective tool to analyze the slope stability. The simulation results of Rouainia *et al*. (2009) showed that the slope deformation is closely related to climate change i.e., WDCs. Besides, the mechanical response of the slope to pore water pressure changes was modelled by Ridley *et al*. (2004) and Smethurst *et al*. (2006). A number of useful conclusions about the slope stability under WDCs can be drawn from their research. However, there are few studies on the method of computing FOS of soil slope under such conditions. The computation of FOS is one of the major tasks in slope stability analysis.

Over the past decades, many different methods have been developed for calculating the FOS of slope, such as the limit equilibrium method (LEM) and the shear strength reduction finite element method (SSRFEM). The SSRFEM was proposed as early as 1975 by Zienkiewicz *et al*. (1975) and has since been applied by Donald and Giam (1988), Matsui and San (1992), Ugai and Leshchinsky (1995), Dawson *et al*. (1999), Griffiths and Lane (1999), Zheng *et al*. (2006), and others. The FOS of the slope can be easily calculated only through reducing effective cohesion (c') and tangent of effective friction angle ($\tan\varphi'$) in equal proportion with the finite element method (FEM). In addition, the distributions of stress, strain and displacement in the slope can be obtained. Most importantly, this method is applicable to a variety of complex geometry, boundary and loading conditions. Thus, SSRFEM is increasingly used for estimating the FOS of slope. However, this method that reduces c' and $\tan\varphi'$ in the same proportion may not be applicable to the slope under conditions of WDCs, because the influence of WDCs on c' and $\tan\varphi'$ may be different. In order to apply this method to the slope under WDCs thus, it is necessary to make some proper modifications for it.

To modify SSRFEM, the influence of WDCs on the parameters of shear strength and stiffness of soils should be analyzed primarily. In fact, some laboratory experiments have been undertaken to investigate the impact of WDCs on the properties of soil. Rajiaram and Erbach (1999), Uchaipichat (2010) and Goual *et al*. (2011) studied the influence of WDCs on physical properties of clay and tuff-calcareous sand mixture, including bulk density, cone penetration resistance, shear strength, adhesion and aggregate. The strength characteristics of unsaturated soil and cement-stabilized silty clay under multiple WDCs were investigated by Goh *et al*. (2014), Suksun *et al*. (2010) and Kampala *et al*. (2014). The effects of WDCs on the swelling potential of clay, sand-bentonite mixture, lime-stabilized soil and silica-fume-stabilized soil were investigated in several studies by Guney *et al*. (2007), Kalkan *et al*. (Kalkan and Akbulut 2004, Kalkan 2009, 2011), Ahmadi *et al*. (2012), Akcanca and Aytekin (2012) and Wang *et al*. (2014). Besides, Chen and Ng (2013) studied the impact of WDCs on the hydro-mechanical behavior of unsaturated soils. Estabragh *et al*. (2013) investigated the effect of different types of wetting fluids (distilled water, saline water and acidic water) on the wetting and drying behaviour of clay soil. The impacts of WDCs on many physical and mechanical properties were investigated by these researchers, but seldom studies were related to the parameters of shear strength and stiffness that determine the FOS of slope.

The main objective of this research is to modify the conventional SSRFEM to estimate the FOS of the soil slope under WDCs. A series of WDCs tests and triaxial tests were carried out to explore the influence of WDCs on the shear strength, effective cohesion, effective internal friction angle and secant modulus of elasticity. Based on the test results, a modified SSRFEM was proposed. Finally, the modified method was applied to calculate the FOS of a slope example under WDCs.

2. Materials and methods

2.1 Soil

The soil utilized in the tests was obtained from a foundation pit in Chongqing, a city in southwest of China. To reduce disturbance, several soil cubes nearly sized of 200 × 200 × 200 mm were excavated at the site. Marked with the vertical direction, the cubes were sealed with plastic paper and packed into boxes, and then taken back to the laboratory carefully, as shown in Fig. 1.

Laboratory tests such as natural density, natural water content, specific gravity, liquid limits, plastic limit and void ratio were performed. Table 1 presents some physical properties of the soil, using the relevant tests according to the ASTM standard. The liquid limit was 39%, the plastic limit was 19% and the specific gravity of the solid was 2.73. According to the Casagrande Plasticity Chart and the Unified Soil Classification System (USCS), the soil was the silty clay.

The mineral composition of the soil was analyzed by X-ray diffraction (XRD). The instrument used in the XRD is D8 ADVANCE, produced by the BEVKER-axs company in Germany. The 2θ lies in the range of 110°~168° and the angle accuracy is 0.0001°. Fig. 2 shows the XRD material patterns, with the main constituents being Muscovite (37.63%), Quartz (28.39%), Albite (18.15%), Microcline (9.32%), Nontronite (4.08%) and Clinochlore (2.43%).

Table 1 Physical properties of the silty clay

Natural density ρ/kg/m^3	Natural water content w /%	Specific gravity G_s	Liquid limit W_L /%	Plastic limit w_p /%	Void ratio e
1820	20.10	2.73	39	19	0.803

Fig. 1 Soil for test

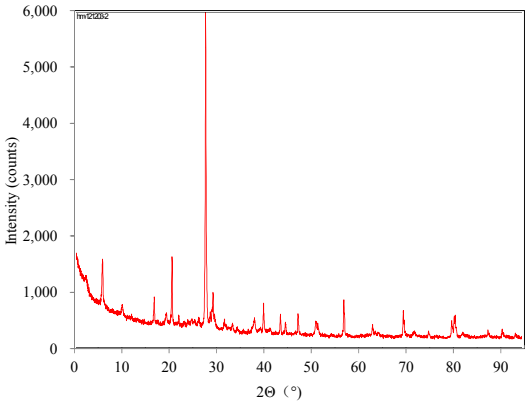

Fig. 2 XRD sample analysis

Fig. 3 Soil samples

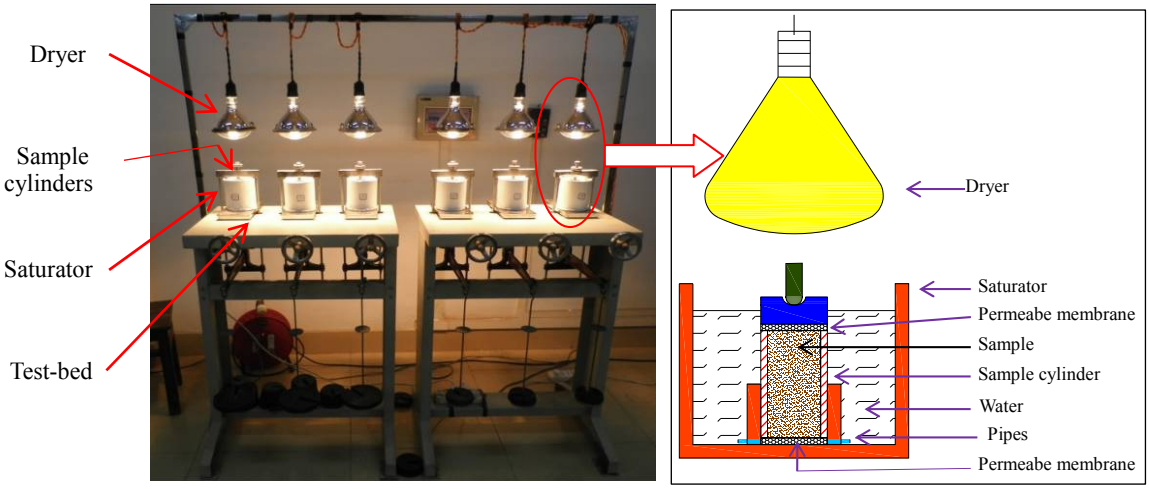

Fig. 4 WDCs test equipment

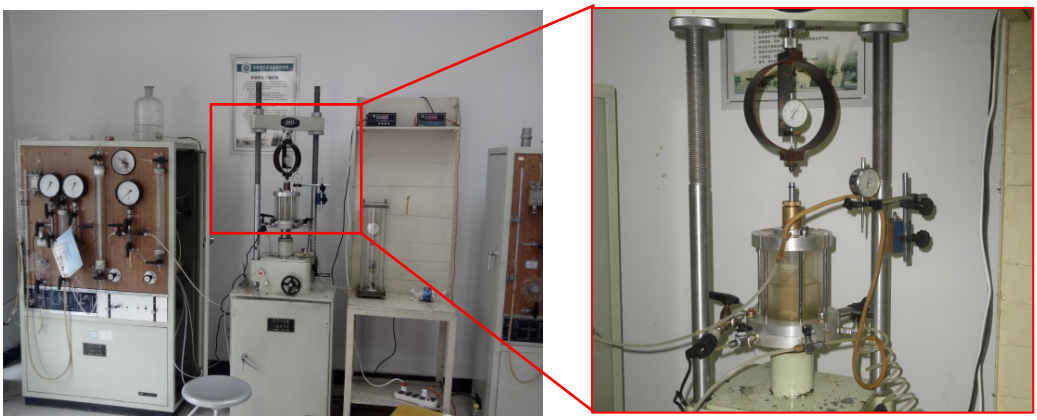

Fig. 5 Triaxial shear test system

2.2 Sample preparation

In order to conduct a precise parametric study, all the undisturbed samples were prepared in the laboratory. In advance, it was necessary to check whether the structure of soil was disturbed. If the soil met the test requirements, twelve cylindrical samples with 80 mm height and 39.1 mm diameter should be prepared by special tools, as shown in Fig. 3.

2.3 Test equipments

The test was composed of two parts: WDCs test and triaxial test. The former test was performed with a self-developed equipment for wetting-drying cycles including test-bed, saturators, dryers and sample cylinders as shown in Fig. 4. The triaxial test was conducted with a SJ-1A triaxial shear system as shown in Fig. 5.

2.4 Test methods

In order to obtain the effects of WDCs on the parameters of shear strength and stiffness of undisturbed silty clay, WDCs test was carried out with four groups which experienced 0.5, 2.5, 4.5 and 8.5 WDCs, respectively. After that, the three soil samples in each group became saturated and they would be sheared in the triaxial shear system.

2.4.1 WDCs test

The FOS of soil slope will decrease to the lowest when the soil is saturated. Heavy rainfall or rising of underground water level can make the soil slope saturated (Mshana *et al*. 1993 and Chandler 1972). Hence, the samples were wetted to saturated water content (29.36%) with saturators and then dried to initial water content (20.10%) with dryers during WDCs.

In order to control the change of water content in *WDCs* test, the method of setting regular drying time and wetting time was adopted by Estabragh *et al*. (2013), Aldaood *et al*. (2014) and Kampala *et al*. (2014). This method was also used in this *WDCs* test. However, the relationship between the water content and wetting-drying time is unknown. It is necessary, therefore, to find this relationship. First, three samples were loaded in the cylinders of the *WDCs* test equipment referring to Fig. 4. The water is then poured into the saturators until the water level is higher than the top surface of the samples as shown in Fig. 6. At this time, the samples were in the process of wetting. The relationship between the water content and wetting time can be obtained by measuring the weight of the samples at a time interval in this process. When the weight of the samples was no longer changing, the wetting process was completed. The water in the saturators would be drained with the pipe, and the dryers would be opened as shown in Fig. 6. At this time, the samples were in the process of drying. The weight of the samples was measured at a time interval in this process to investigate the relationship between the water content and drying time. Hence, this relationship was obtained, as shown in Fig. 7. It shows that the variation law of the three samples is not exactly the same, but the difference between them is very little. As a result, their average value can be used as a standard to control the change of water content in *WDCs* test. The method of setting regular drying time and wetting time to control the change of water content may have some errors, but the researches by Estabragh *et al*. (2013), Aldaood *et al*. (2014) and Kampala *et al*. (2014) show that the effects of such error on *WDCs* test is very small. This error can be neglected in the paper.

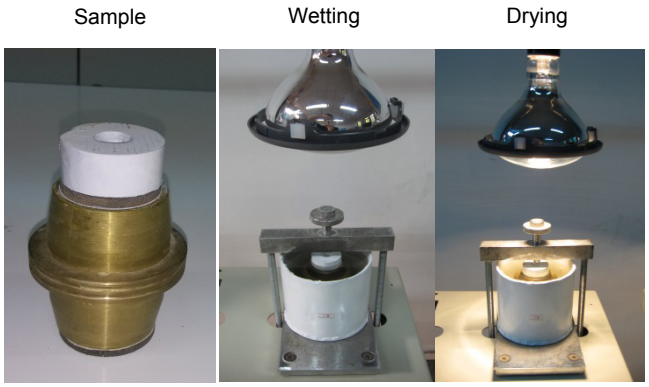

Fig. 6 Wetting and drying samples

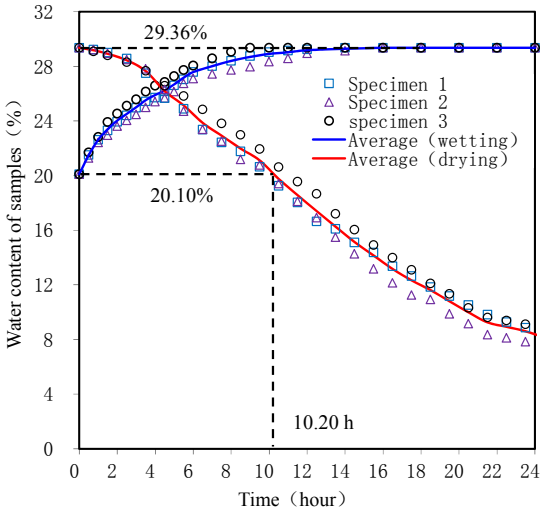

Fig. 7 The relationship between the water content of samples and wetting-drying hours

Thus, in order to keep the water content cycling between 20.10% and 29.36%, the *WDCs* test equipment should be in the state of 24 hours' wetting and 10.2 hours' drying. Fig. 8 shows the water content during 2.5 *WDCs*. It needed 34.2 hours for one cycle.

2.4.2 Consolidated undrained triaxial test

After the *WDCs* test, the consolidated undrained (CU) triaxial test was conducted. 24 hours is enough for the samples to complete consolidation. Three saturated samples of each group were sheared at the rate of 0.077 mm/min in triaxial shear system with confining pressures of 50 kPa, 100 kPa and 200 kPa (σ_3 = 50 kPa, σ_3 = 100 kPa and σ_3 = 200 kPa), respectively. In the triaxial test, four readings must be recorded carefully, including volume deformation, dial indicator of stress ring, axial deformation and pore water pressure. When the axial strain (ε_1) reaches 15%, the test was completed. Fig. 9 shows the twelve damaged samples after triaxial test. The sample on the left side of the picture is a standard sample.

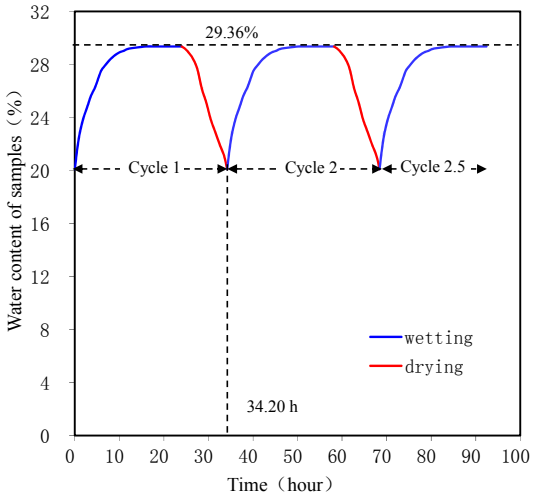

Fig. 8 Water content of samples during 2.5 *WDCs*

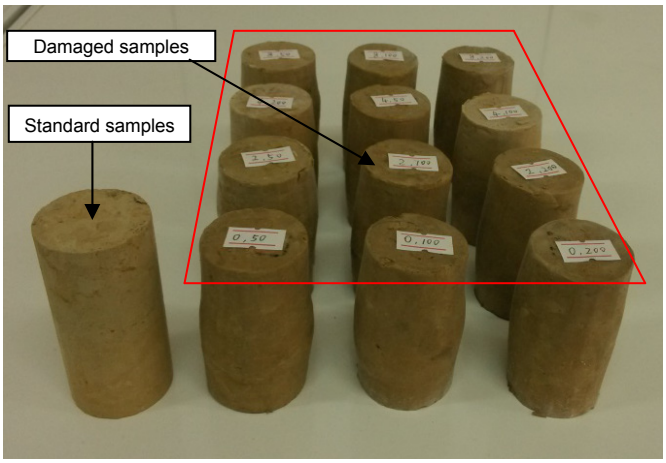

Fig. 9 Damaged samples after triaxial test

3. Results and analysis

3.1 Effect of WDCs on shear strength

Through the triaxial test, the stress-strain curves of the samples under the conditions of different σ_3 and different number of *WDCs* can be obtained, as shown in Figs. 10(a), (b), (c) and (d). These curves can be divided into three regions. Region I is elastic region. When the axial strain is very little, the stress increases linearly with the increasing axial strain. Region II is elastic-plastic region. Since the strain in this region includes elastic strain and plastic strain, the stress rises nonlinearly with the increasing axial strain. Region III is plastic region. In this region, the stress gets few changes, which means that the strain is plastic strain. Therefore, the constitutive relation of silty clay is similar to Duncan-Chang model.

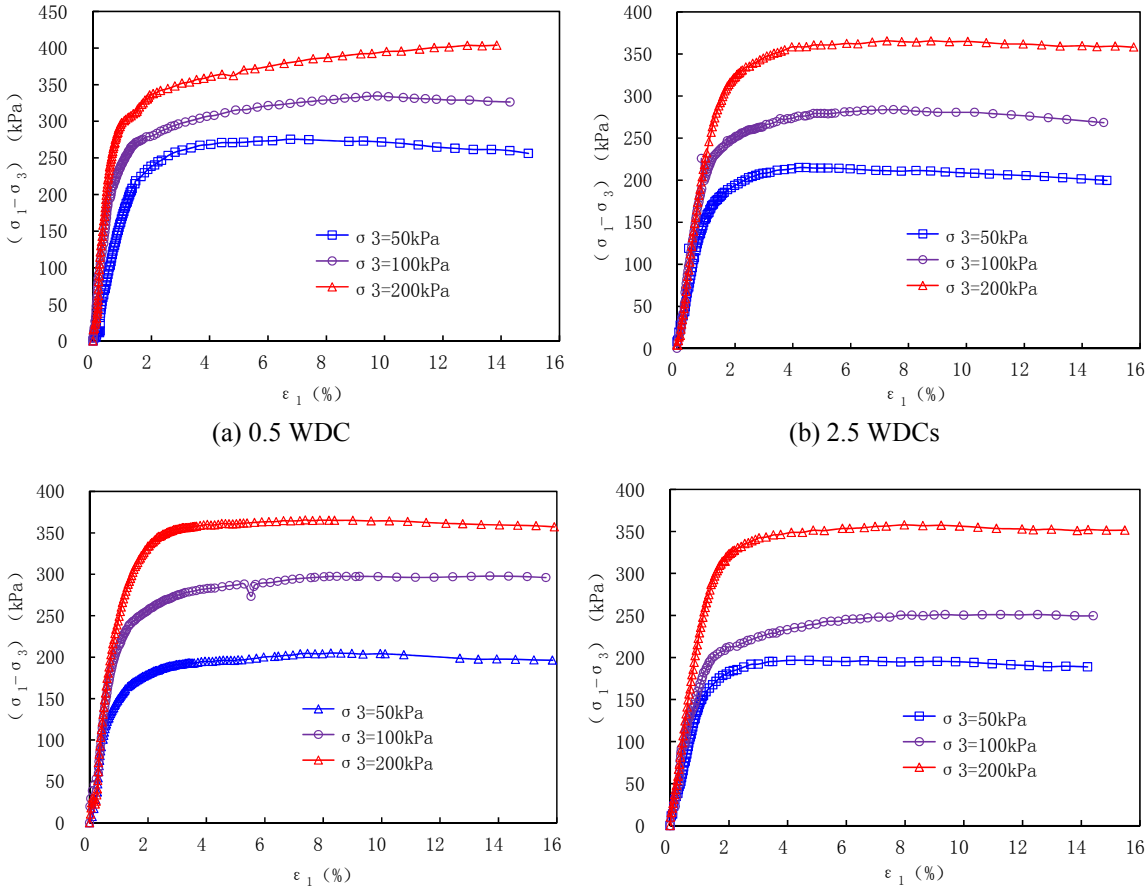

(a) 0.5 WDC (b) 2.5 WDCs

(c) 4.5 WDCs (d) 8.5 WDCs

Fig. 10 Stress-strain curves of the samples

Table 2 Shear strength of the samples (*kPa*)

Cycles /times	0.5	2.5	4.5	8.5
σ_3 = 50 kPa	275.46	214.94	203.92	196.58
σ_3 = 100 kPa	334.61	283.79	297.86	251.16
σ_3 = 200 kPa	403.58	365.48	365.07	357.75

The shear strength $((\sigma_1 - \sigma_3)_f)$ is the peak value in the stress-strain curves. When there is no obvious peak value in the curves, the $(\sigma_1 - \sigma_3)$ corresponding to ε_1 = 15% can be used as the peak value according to the ASTM standard. Thus, the shear strength that varies with σ_3 and the number of *WDCs* can be obtained from the peak values in Fig. 10, as shown in Table 2. Fig. 11 shows the relation curves between $(\sigma_1 - \sigma_3)_f$ and the number of *WDCs* under different confining pressures. The shear strength increases with the increasing of confining pressure and decreases with the increasing number of *WDCs*. The conclusion comes to be that *WDCs* have a degradation effect on the shear strength of undisturbed silty clay.

Table 3 Shear strength parameters of samples

Cycles /times	0.5	2.5	4.5	8.5
c'/kPa	83.10	62.10	59.48	49.62
$\eta_{c'}$	1.00	0.75	0.72	0.60
φ'/°	18.96	19.37	20.00	20.71
$\eta_{\varphi'}$	1.00	1.02	1.04	1.04

3.2 Effects of WDCs on c' and φ'

The shear strength parameters (effective cohesion c' and effective internal friction angle φ') under the condition of different number of *WDCs* are shown in Table 3. The relation curves between coefficient η and the number of *WDCs* are shown in Fig. 12 where $\eta_{c'}$ and $\eta_{\varphi'}$ can be calculated as Eq. (1)

$$\eta_{c'} = \frac{c'}{c'_0}, \quad \eta_{\varphi'} = \frac{\tan\varphi'}{\tan\varphi'_0}, \tag{1}$$

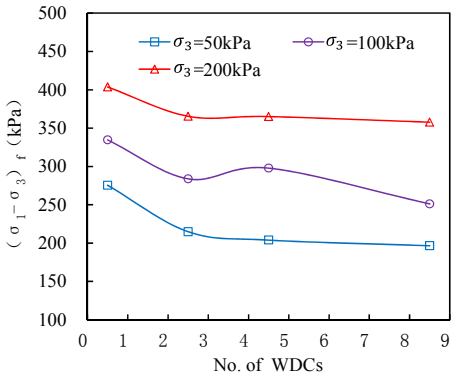

Fig. 11 $(\sigma_1 - \sigma_3)_f$ varies with σ_3 and the No. of *WDCs*

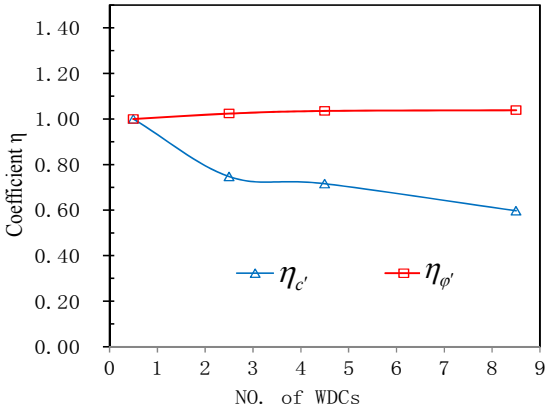

Fig. 12 Coefficient η vs No. of *WDCs*

where c'_0 is the initiative effective cohesion and φ'_0 is the initiative effective internal friction angle; c' and φ' are effective cohesion and effective internal friction angle after *WDCs* test.

Fig. 12 shows that c' decreases greatly with the increasing number of *WDCs*, especially after the first 2.5 cycles, while tanφ' remains constant. Thus, *WDCs* have a great effect on c', but few effects on tanφ' of undisturbed silty clay.

3.3 Effect of WDCs on E_s

In order to study the effect of *WDCs* on stiffness parameter of silty clay, secant modulus of elasticity (E_s) is defined, as shown in Eq. (2). E_s is the slope of secant drawn from the origin to the point of 50% $(\sigma_1 - \sigma_3)_f$ in stress-axial strain curve. It reflects the average stiffness of soil.

$$E_s = \frac{50\%(\sigma_1 - \sigma_3)_f}{\varepsilon_1} \tag{2}$$

where $(\sigma_1 - \sigma_3)_f$ is the peak shear strength; ε_1 is the axial strain corresponding to the point of 50% $(\sigma_1 - \sigma_3)_f$.

E_s that varies with σ_3 and the number of *WDCs* can be obtained from the stress-strain curves in Fig. 10, as shown in Fig. 13. It shows that E_s increases with the increasing of σ_3 and decreases with the increasing number of *WDCs*. Thus, *WDCs* have a degradation effect on the secant modulus of elasticity of undisturbed silty clay.

3.4 Analysis

WDCs have a degradation effect on shear strength and secant modulus of elasticity, which is caused by two factors. On the one hand, undisturbed silty clay containing clay minerals has the potential for swelling and shrinkage under *WDCs* conditions (Kalkan and Akbulut 2004, Kalkan 2009, 2011). *WDCs* can cause progressive deformation of silty clay and development of cracks, which can reduce the cementation among clay particles and destroy the structure of soil to make it looser (Malusis *et al*. 2011). Therefore, shear strength, effective cohesion and secant modulus of elasticity all decrease. On the other hand, during *WDCs*, some small clay particles inside the silty

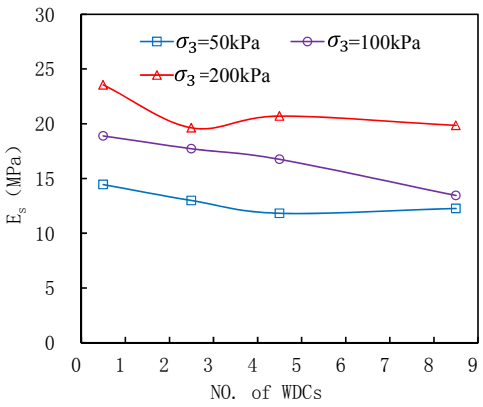

Fig. 13 E_s varies with No. of WDCs and σ_3

clay gather to be bigger ones with the Van der Waals forces, which increase the effective friction among soil particles (Kholodov 2013). Thus, both sides can make sense that *WDCs* have little influence on effective internal friction angle.

4. Modifications to SSRFEM

4.1 Definition of the FOS

When the Mohr-Coulomb failure criterion is used, the shear strength is expressed as Eq. (3).

$$\tau_f = c' + \sigma_n \tan\varphi' \tag{3}$$

where the cohesion c' and the internal friction angle φ' are two effective shear strength parameters. With the SSRFEM, the shear strength is decreased by reducing the values of the two shear strength parameters, that is

$$c_r = c' / SRF_c \tag{4a}$$

$$\tan\varphi_r = \tan\varphi' / SRF_\varphi \tag{4b}$$

where SRF_c and SRF_φ are the strength reduction factors corresponding to the effective cohesion and effective internal friction angle, respectively, and it is usually assumed that $SRF_c = SRF_\varphi = SRF$.

The *WDCs* test and triaxial test expose that the shear strength of undisturbed silty clay is decreased with the increasing number of *WDCs*. Therefore, it can be concluded that the basic reason for silty clay slope failure subjected to *WDCs* is that the shear strength and stiffness of silty clay degrade. This is similar to the definition of the FOS in Eq. (4) based on the SSRFEM. Thus, Eq. (4) can be used as a definition of the FOS of the soil slope which is mainly affected by *WDCs*.

The tests results show that c' and $\tan\varphi'$ change differently under the condition of *WDCs* in which c' decreases rapidly and $\tan\varphi'$ remains constant. Obviously, according to the definition of the FOS in SSRFEM, c' and $\tan\varphi'$ reduced in the same proportional do not comply with the test results. In accordance with the test results, the most appropriate method to compute the FOS of silty clay slope under *WDCs* is only to reduce c' without $\tan\varphi'$, as shown in Eq. (5)

$$c_r = c' / SRF_c \tag{5a}$$

$$\tan\varphi_r = \tan\varphi' \tag{5b}$$

Thus, SRF_c at the transitionpoint from stablility to failure can be defined as the FOS of slope under *WDCs*, that is, $FOS = SRF_c$.

4.2 Reduction of elastic modulus

When computing the FOS of slope with conventional SSRFEM, only the strength parameters get reduced, while the stiffness parameters do not need to reduce (Zienkiewicz *et al*. 1975).

However, The E_s of silty clay will decrease under *WDCs*. Therefore, the stiffness parameters should be also reduced when taking SSRFEM to compute the FOS.

The stress-strain curves of the samples in this test approximately comply with Duncan-Chang model whose expressions are shown in Eqs. (6), (7), (8), (9), (10). The relationship between strength parameters c', φ' and the deformation parameters E can be found out by this model (Zhang and Chen 2006).

$$E_t = [1 - R_f S]^2 E_i \tag{6}$$

$$E_i = k\left(\frac{\sigma_3}{p_a}\right)^n \tag{7}$$

$$R_f = \frac{(\sigma_1 - \sigma_3)_f}{(\sigma_1 - \sigma_3)_{ult}} \tag{8}$$

$$S = \frac{\sigma_1 - \sigma_3}{(\sigma_1 - \sigma_3)_f} \tag{9}$$

$$(\sigma_1 - \sigma_3)_f = \frac{2c' \cdot \cos\varphi' + 2\sigma_3 \cdot \sin\varphi'}{1 - \sin\varphi'} \tag{10}$$

where E_t is the tangent elasticity modulus; E_i is the initial tangent elasticity modulus; R_f is the ratio between the shear strength $(\sigma_1 - \sigma_3)_f$ and ultiate shear strength $(\sigma_1 - \sigma_3)_{ult}$; S is the stress level which shows the ratio between actual stress $\sigma_1 - \sigma_3$ and shear strength $(\sigma_1 - \sigma_3)_f$; Pa is the standard atmospheric pressure of 1.013×10^5 Pa.

Substituting Eqs. (7), (8), (9) and (10) into Eq. (6) gives

$$E_t = \left[1 - R_f \frac{(\sigma_1 - \sigma_3)(1 - \sin\varphi')}{2c' \cdot \cos\varphi' + 2\sigma_3 \cdot \sin\varphi'}\right]^2 E_i \tag{11}$$

In Eq. (11), R_f, E_i and $(\sigma_1 - \sigma_3)$ are constant, but c' and $\tan\varphi'$ will be reduced with the increasing of *SRF*. Thus, E_t can be reduced with the decreasing of c' and $\tan\varphi'$ based on Eq.(11).

5. Example

5.1 Slope profile

The slope is located in Sichuan Province in China, higher in the east and lower in the west. There are two kinds of formation lithology: silty clay in the upper layer and mudstone in the lower layer. In front of the slope, there is a lake whose water level rising and falling periodically, as shown in Fig. 14. Located in semi-tropical humid monsoon climate zone at the northeast edge of Sichuan Basin, the slope experiences four distinct seasons, rainy summer and arid winter. Thus, the slope is under conditions of *WDCs*.

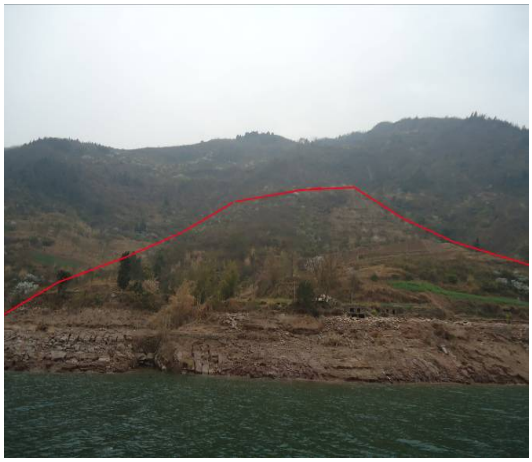

Fig. 14 View of the slope

Table 4 Physical properties of the materials

Material	*c' /kPa*	*φ' / °*	*E /MPa*	*v*	*ρ /kg/m³*
Silty clay	30.2	15.8	63	0.38	2040
Mudstone	4730	40.5	4557	0.30	2640

According to the geological exploration data of the slope, the properties of the materials are obtained, as shown in Table 4.

5.2 Slope model

The soil slope is simplified to a plane strain model including 14375 elements and 14553 nodes in finite difference program FLAC 5.00 (Itasca Consulting Group, Inc. 2002), as shown in Fig. 15.

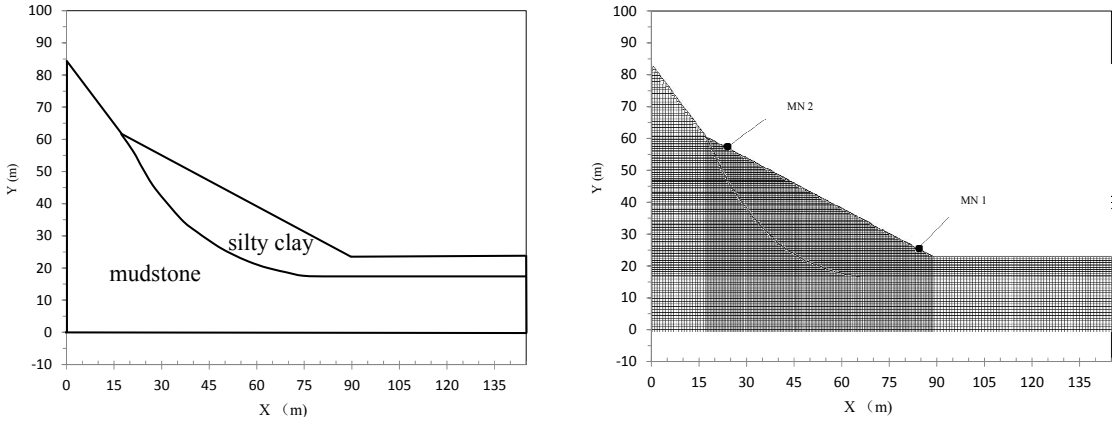

(a) Geometry (b) Finite element mesh

Fig. 15 Slope model in FLAC

Its X-displacements were fixed for nodes along the left and right boundaries, while all displacements were fixed along the bottom boundary. The slope face was kept free. The marked node 1 (MN 1) is at the slope toe and marked node 2 (MN 2) at the slope crest. The FOS of the slope is computed with the adjusted SSRFEM which is proposed in the previous paper. In other words, only cohesion c' and elastic modulus E are reduced based on Eq.(5) and Eq.(11), respectively.

5.3 Results and analysis

When applying the SSRFEM to compute the FOS, three behaviours can be utilized to identify the occurrence of slope failure, namely, non-convergence of the nonlinear iterative method (behaviour I), a plastic zone going through the slope from the toe to the top (behaviour II) and sudden substantial changes in the displacement of marked nodes (behaviour III) (Griffiths and Lane 1999, Dawson *et al*. 1999 and Manzari and Nour 2000). Consequently, *SRF* at the transitionpoint from stability to failure can be defined as the FOS, that is, $FOS = SRF$.

SRF_c at the transitionpoint from convergence to non-convergence of the nonlinear iterative method is 1.22. Hence, the FOS is 1.22 judged by the behavior I.

Fig. 16 shows the plastic shear band in slope when the SRF_c is 1.20 and 1.22, respectively. When SRF_c grows from 1.20 to 1.22, the plastic shear band at the toe of the slope connects with the plastic shear band at the top of the slope. It is the critical state of the slope, so the FOS of the slope is 1.22 judged by the behavior II.

According to the numerical modeling results, the relation curves between the SRF_c and the displacement (S) of MN 1 and MN 2 are shown in Fig. 17. Both the X-displacement of MN 1 (S_x-MN 1) and Y-displacement of MN 2 (S_y-MN 2) increase substantially in a sudden when the SRF_c grows from 1.24 to 1.26. The catastrophe points (CP) at the curves of S-SRF_c are SRF_c = 1.24. Hence, the FOS is 1.24 based on behaviour III.

Since there seems not to be a distinct catastrophe point at curves of S-SRF_c, the FOS is hard to estimate. There is a new behaviour which is similar to behavior III. In order to judge the CP at the curves of S-SRF_c accurately, the curves of $\Delta S/\Delta SRF_c$-SRF_c can be plotted as Fig. 18. These curves

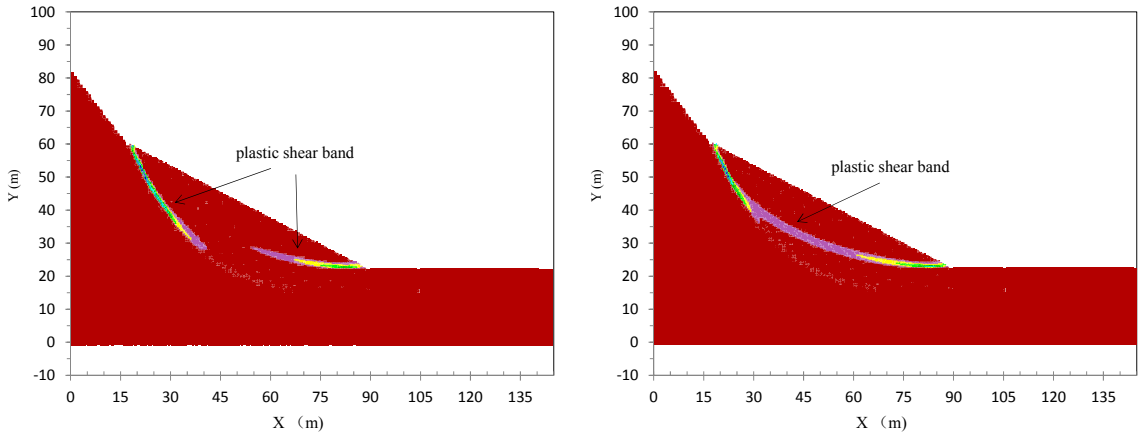

(a) SRF_c = 1.20 (b) SRF_c = 1.22

Fig. 16 Plastic shear band in slope model

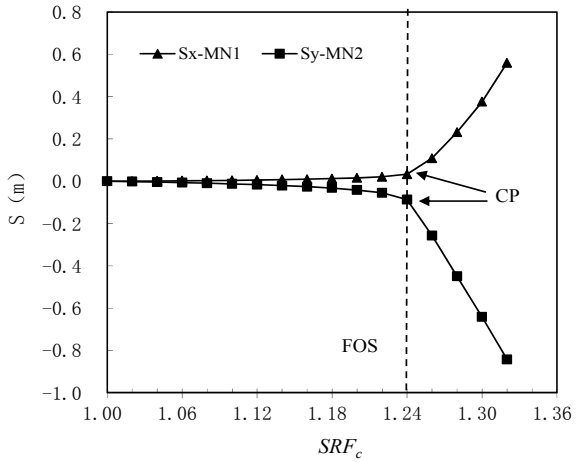

Fig. 17 *S*-SRF_c curves of marked node1 and maked node 2

show the relationship between SRF_c and $\Delta S/\Delta SRF_c$ which is the gradients of *S*-SRF_c curves. When SRF_c < 1.22, the curves of $\Delta S/\Delta SRF_c$-SRF_c are almost straight horizontal lines. However, the curves appear to be catastrophes when SRF_c increases to 1.24. Hence, the behavior that sudden substantial changes of $\Delta S/\Delta SRF_c$ at the curves of $\Delta S/\Delta SRF_c$-SRF_c can be used to identify the occurrence of slope failure (behaviour IV). The FOS of the slope is 1.24 based on behaviour IV.

Compared with the behaviour III, the behaviour IV possesses some advantages. On the one hand, as the increase of SRF_c, the large displacement of MN doesn't mean the slope will slip or the SRF_c is the FOS, but the abrupt increment of $\Delta S/\Delta SRF_c$ does mean that the displacement is greatly influenced by SRF_c. In other words, if SRF_c increases little, the large increment of the displacement of MN means the slope will slip. Thus, the behaviour IV reflects the nature of slope failure. On the other hand, the catastrophe point at the $\Delta S/\Delta SRF_c$-SRF_c curves is easier to confirm, which can make FOS more accurate.

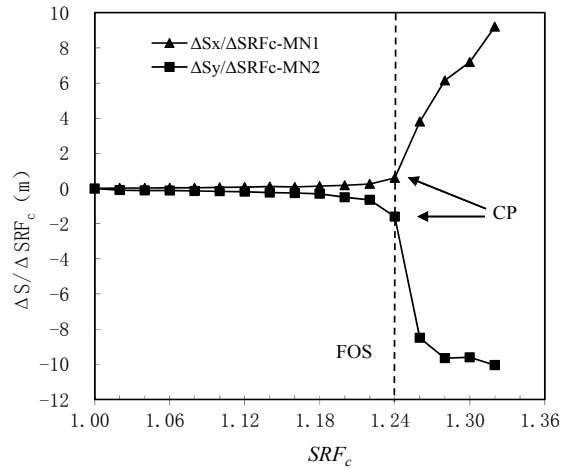

Fig. 18 $\Delta S/\Delta SRF_c$-SRF_c curves of maked node1 and maked node 2

Based on behaviour I, II, III and IV, the FOS of the slope is 1.22, 1.22, 1.24 and 1.24, respectively. Thus, the FOS of the slope can be estimated between 1.22 and 1.24 under WDCs.

6. Conclusions

A series of *WDCs* tests and triaxial tests were carried out to investigate the influence of *WDCs* on the parameters of shear strength and stiffness. Based on the test results, the conventional SSRFEM was modified to calculate the FOS of soil slope under *WDCs*. The main conclusions of this paper can be drawn as follows:

- With the increasing number of *WDCs*, the shear strength ($(\sigma_1 - \sigma_3)_f$), effective cohesion (c') and secant modulus of elasticity (E_s) all decrease, while effective friction angle (φ') remains constant. Consequently, *WDCs* have a degradation effect on $(\sigma_1 - \sigma_3)_f$, c' and E_s.
- The degradation effect of *WDCs* is caused by two factors. On the one hand, *WDCs* destroy the structure of soil to make it looser. On the other hand, some small clay particles inside the silty clay gather to be bigger ones which increase the effective friction among soil particles.
- For *WDCs* have a degradation effect on c' while little influence on $\tan\varphi'$, conventional SSRFEM which reduces c' and $\tan\varphi'$ in equal proportion cannot be adopted to compute the FOS of soil slopes under *WDCs*. Thus, the SSRFEM should be modified. In detail, c' is merely reduced among shear strength parameters, and E is reduced correspondingly.
- Sudden substantial changes of the displacements of marked nodes (behaviour III) can be utilized to identify the occurrence of slope failure. Based on behavior III, a new behavior is proposed to identify the slope failure.
- The modified SSRFEM is applied to compute the FOS of a slope example under *WDCs* located in Sichuan Province in China. The modelling result shows that the FOS of the slope can be estimated between 1.22 and 1.24.

Acknowledgments

The present study was financially supported by the National Natural Science Foundation of China (Grant No. 51108485 and 41372356), the Specialized Research Fund for the Doctoral Program of Higher Education of China (Grant No. 20110191120033) and the Fundamental Research Funds for the Central Universities of China (Grant No. CDJZR 12200012).

References

Ahmadi, H., Rahimi, H. and Rostami, M.E. (2012), "Control of swelling of soil under canal lining by wetting and drying cycles", *Irrig. Drain.*, **61**(4), 527-532.

Akcanca, F. and Aytekin, M. (2012), "Effect of wetting–drying cycles on swelling behavior of lime stabilized sand–bentonite mixtures", *Environ. Earth Sci.*, **66**(1), 67-74.

Al-Mukhtar, M., Khattab, S. and Alcover, J.F. (2012), "Microstructure and geotechnical properties of lime-treated expansive clayey soil", *Eng. Geol.*, **139-140**, 17-27.

Aldaood, A., Bouasker, M. and Al-Mukhtar, M. (2014), "Impact of wetting–drying cycles on the microstructure and mechanical properties of lime-stabilized gypseous soils", *Eng. Geol.*, **174**, 11-21.

Brooks, S.M., Crozier, M.J. and Glade, T.W. (2004), "Towards establishing climatic thresholds for slope instability: use of a physically-based combined soil hydrology-slope stability model", *Pure Appl.*

Geophys., **161**(4), 881-905.
Chandler, R.J. (1972), "Lias clay: Weathering processes and their effect on shear strength", *Geotechnique*, **22**(3), 403-431.
Chen, R. and Ng, C.W.W. (2013), "Impact of wetting–drying cycles on hydro-mechanical behavior of an unsaturated compacted clay", *Appl. Clay Sci*., **86**, 38-46.
Clarke, D. and Smethurst, J.A. (2010), "Effects of climate change on cycles of wetting and drying in engineered clay slopes in England", *Quarter. J. Eng. Geol. Hydrogeol*., **43**(4), 473-486.
Dawson, E.M., Roth, W.H. and Drescher, A. (1999), "Slope stability by strength reduction", *Geotechnique*, **49**(6), 835-840.
Donald, I.B. and Giam, S.K. (1988), "Application of the nodal displacement method to slope stability analysis", *Proceedings of the 5th Australia-New Zealand Conference on Geomechanics*, Sydney, Australia, August.
Estabragh, A.R., Moghadas, M. and Javadi, A.A. (2013), "Effect of different types of wetting fluids on the behavior of expansive soil during wetting and drying", *Soils Found*., **53**(5), 617-627.
Goh, S.G., Rahardjo, H. and Leong, E.C. (2014), "Shear strength of unsaturated soils under multiple drying-wetting cycles", *J. Geotech. Geoenviron. Eng.-ASCE*, **140**(2), 06013001-06013005.
Goual, I., Goual, M.S. and Taibi, S. (2011), "Behaviour of unsaturated tuff-calcareous sand mixture on drying-wetting and triaxial paths", *Geomech. Eng*., *Int. J*., **3**(4), 267-284.
Griffiths, D.V. and Lane, P.A. (1999), "Slope stability analysis by finite elements", *Geotechnique*, **49**(3), 387-403.
Gullà, G., Mandaglio, M.C. and Moraci, N. (2006), "Effect of weathering on the compressibility and shear strength of a natural clay", *Can. Geotech. J*., **43**(6), 618-625.
Guney, Y., Sari, D., Cetin, M. and Tuncan, M. (2007), "Impact of cyclic wetting–drying on swelling behavior of lime-stabilized soil", *Build. Environ*., **42**(2), 681-688.
Hughes, P.N., Glendinning, S. and Mendes, J. (2009), "Full-scale testing to assess climate effects on embankments", *Proceedings of the Institution of Civil Engineers-Engineering Sustainability*, **162**(2), 67-79.
Itasca Consulting Group, Inc. (2002), FLAC–Fast Lagrangian Analysis of Continua, Version 4.0 Users' Guide, Itasca, Consulting Group, Inc., Minneapolis, MN, USA.
Kalkan, E. (2009), "Influence of silica fume on the desiccation cracks of compacted clayey soils", *Appl. Clay Sci*., **43**(3-4), 296-302.
Kalkan, E. (2011), "Impact of wetting–drying cycles on swelling behavior of clayey soils modified by silica fume", *Appl. Clay Sci*., **54**(4), 345-352.
Kalkan, E. and Akbulut, S. (2004), "The positive effects of silica fume on the permeability, swelling pressure and compressive strength of natural clay liners", *Eng. Geol*., **73**(1-2), 145-156.
Kampala, A., Horpibulsuk, S., Prongmanee, N. and Chinkulkijniwat, A. (2014), "Influence of wet-dry cycles on compressive strength of calcium carbide residue–fly ash stabilized clay", *J. Mater. Civil Eng*., **26**(4), 633-643.
Kholodov, V.A. (2013), "The capacity of soil particles for spontaneous formation of macro aggregates after a wetting-drying cycle", *Eurasian Soil Sci*., **46**(6), 660-667.
Kilsby, C., Glendinning, S. and Hughes, P.N. (2009), "Climate-change impacts on long-term performance of slopes", *Proceedings of the Institution of Civil Engineers-Engineering Sustainability*, **162**(2), 59-66.
Leroueil, S. (2001), "Natural slopes and cuts: movement and failure mechanisms", *Géotechnique*, **51**(3), 197-243.
Malusis, M.A., Yeom, S. and Evans, J.C. (2011), "Hydraulic conductivity of model soil-bentonite backfills subjected to wet-dry cycling", *Can. Geotech. J*., **48**(8), 1198-1211.
Manzari, M.T. and Nour, M.A., (2000), "Significance of soil dilatancy in slope stability analysis", *J. Geotech. Geoenviron. Eng*., **123**(1), 75-80.
Matsui, T. and San, K.C. (1992), "Finite element slope stability analysis by shear strength reduction technique", *Soils Found*., **32**(1), 59-70.
Mshana, N.S., Suzuki, A. and Kitazono, Y. (1993), "Effects of weathering on stability of natural slopes in

north-central Kumamoto", *Soils Found*., **33**(4), 74-87.
Nowamooz, H., Jahangir, E. and Masrouri, F. (2013), "Volume change behaviour of a swelling soil compacted at different initial states", *Eng*. *Geol*., **153**, 25-34.
Rajiaram, G. and Erbach, D.C. (1999), "Effect of wetting and drying on soil physical properties", *J*. *Terramech*., **36**(1), 39-49.
Ridley, A., McGinnity, B. and Vaughan, P. (2004), "Role of pore water pressures in embankment stability", *Geotech*. *Eng*., **157**(4), 193-198.
Rouainia, M., Davies, O. and Brien, T.O. (2009), "Numerical modelling of climate effects on slope stability", *Proceedings of the Institution of Civil Engineers-Engineering Sustainability*, **162**(2), 81-89.
Smethurst, J.A., Clarke, D. and Powrie, W. (2006), "Seasonal changes in pore water pressure in a grass-covered cut slope in London Clay", *Geotechnique*, **56**(8), 523-537.
Suksun, H., Runglawan, R. and Avirut, C. (2010), "Analysis of strength development in cement-stabilized silty clay from microstructural considerations", *Construct*. *Build*. *Mater*., **24**(10), 2011-2021.
Toll, D.G., Mendes, J. and Augarde, C.E. (2008), "Effects of climate change on slopes for transportation infrastructure", *Proceedings of the 1st International Conference on Transportation Geotechnics*, Nottingham, England, August.
Uchaipichat, A. (2010), "Experimental investigation on loading collapse curve of unsaturated soils under wetting and drying processes", *Geomech*. *Eng*., *Int*. *J*., **2**(3), 203-211.
Ugai, K. and Leshchinsky, D. (1995), "Three-dimensional limit equilibrium and finite element analysis: a comparison of results", *Soils Found*., **35**(4), 1-7.
Wang, J.B., Liu, X.R. and Liu, X.J. (2014), "Creep properties and damage model for salt rock under low-frequency cyclic loading", *Geomech*. *Eng*., *Int*. *J*., **7**(5), 569-587.
Zhang, P.W. and Chen, Z.Y. (2006), "Influences of soil elastic modulus and Poisson's ratio on slope stability", *Rock Soil Mech*., **27**(2), 299-303. [In Chinese]
Zheng, H., Tham, L.G. and Liu, D. (2006), "On two definitions of the factor of safety commonly used in the finite element slope stability analysis", *Comput*. *Geotech*., **33**(3), 188-195.
Zienkiewicz, O.C., Humpheson, C. and Lewis, R.W. (1975), "Associated and non-associated visco-plasticity and plasticity in soil mechanics", *Geotechnique*, **25**(4), 671-689.

CC